JMEMS Letters

Linear-Stiffness Rotary MEMS Stage

Utku Baran, Wyatt O. Davis, Sven Holmström, Dean Brown, Jaibir Sharma, Sertan Kutal Gokce, and Hakan Urey

***Abstract*—A novel bending flexure spring design is presented, providing linear stiffness for large rotations of a suspended body. Over 98% linear motion for up to $\pm 7^\circ$ mechanical scan angle is achievable with the new suspension design. [2011-0292]**

***Index Terms*—Comb drive, linear spring, low-frequency laser beam scanning, microelectromechanical systems (MEMS) stage.**

I. Introduction

Large in-plane rotations of a suspended body are desirable for several applications, including optical scanning [1], [2], angular rate sensing [3], [4], tunable lasers [5], optical switchers [6], optical attenuators [7], and compasses [8]. Nonlinear stiffening of the suspension members can limit the quasi-static rotation amplitude that can be achieved with the available forcing amplitude, and so, it is desirable for the suspension members to provide a constant linear stiffness. For microelectromechanical systems (MEMS) devices, micromachined torsion beams are effective at providing linear stiffness for large out-of-plane rotations, but these are not very practical to implement for devices intended to operate in plane. In-plane motion of a MEMS device restricts the suspension design to one using bending flexures. Such flexures will have one end fixed to a substrate and the other end attached to the moving body. The clamped–guided boundary condition will typically result in cubic spring stiffening [9]. This nonlinearity will limit the achievable quasi-static displacement for the forcing amplitude available from the actuator, as demonstrated in [2] and [10], and will produce jump discontinuities and hysteresis in the frequency response (i.e., the classic response characteristics of a Duffing oscillator) [11]. Since the nonlinear stiffening arises from axial tension developing in the suspension beams, previous approaches to managing the nonlinear stiffening for in-plane rotational suspensions have involved introducing extra axial compliance, for example, by flexure folding or meandering, as in [4] and [12], or making the connection to the fixed substrate using a "tee" bending member [2]. These approaches will reduce but not eliminate the cubic stiffening.

This letter demonstrates a different approach that seeks to exploit a special case of clamped–guided beams that have identically zero cubic stiffening without folding or attempts to form compliant boundary conditions. Accordingly, in this letter, a novel spring design is introduced to achieve linear in-plane rotary stiffness. The theoretical motivation and a finite-element model are developed in Section II. The device design and fabrication process are described in Section III, and in Section IV, the device is characterized. Finally, Section V provides some concluding remarks, with comments on application for quasi-static laser beam scanning.

Manuscript received October 1, 2011; revised December 7, 2011; accepted December 19, 2011. Subject Editor O. Solgaard.

U. Baran, S. Holmström, J. Sharma, and H. Urey are with the Optical Microsystems Laboratory, Department of Electrical and Electronics Engineering, Koç University, Istanbul 34450, Turkey (e-mail: ubaran@ku.edu.tr; sholmstrom@ku.edu.tr; jaibirsharma@gmail.com; hurey@ku.edu.tr).

W. O. Davis and D. Brown are with Microvision, Inc., Redmond, WA 98052 USA (e-mail: wyatt_davis@microvision.com; dean_brown@microvision.com).

S. K. Gokce was with Koç University, Istanbul 34450, Turkey. He is now with The University of Texas at Austin, Austin, TX 78712 USA.

Color versions of one or more of the figures in this paper are available online at http://ieeexplore.ieee.org.

Digital Object Identifier 10.1109/JMEMS.2011.2182504

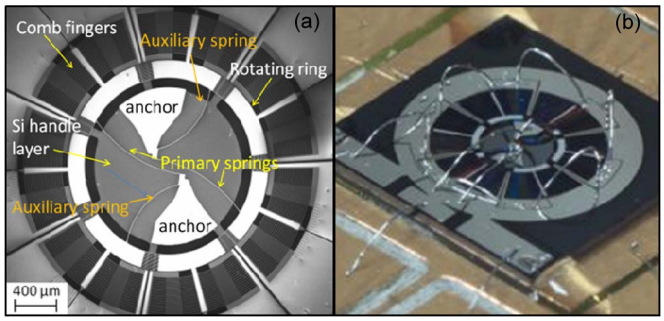

Fig. 1. (a) SE micrograph of the rotary stage. (b) Photograph of a wire-bonded device.

II. Theory

The design goal for the rotating ring suspension is to achieve linear stiffness for large in-plane rotations. Clamped–guided beams will typically exhibit nonlinear stiffening already when the maximum displacement is only a fraction of the beam's width. Exact formulas for the coefficients of cubic stiffening for three cases of clamped–guided boundary conditions were derived in [9] and [13]. It was noted in [13] that the case of a rotating ring with an interior suspension has a vanishing of the cubic stiffness coefficient for two particular ratios of the radius to the length. The exact coefficient of cubic stiffening k_3 for this case is

$$k_3 = \frac{2EA}{225L^3}\left(L^2 - 9LR + 9R^2\right)^2 \tag{1}$$

where E is the elastic modulus, A is the cross-sectional area of the beam, R is the inner radius of the suspended ring, and L is the length. This coefficient is zero for $R/L = 0.87$ and $R/L = 0.13$; however, both of these special cases require suspension beams to cross each other, which makes it impossible to form them out of a single structural layer [13].

Fig. 1(a) shows a scanning electron (SE) micrograph of a microfabricated rotating ring with a rotary comb drive actuator and a suspension that approximates one of these special cases. The anchors for two "primary" beams were positioned near the ideal location $R/L = 0.87$ but with an offset that permitted them to be formed in the same structural layer and to deform without interfering with each other. This offset results in a nonzero k_3; however, a curvature was introduced and fine tuned using finite-element analysis until the desired linearity was recovered. Furthermore, two additional "auxiliary" suspension beams sharing the anchors were added to suppress the tendency of the ring to undergo out-of-plane torsion. The dimensions and the curvature of these auxiliary beams were also designed for the stiffness to remain linear over the desired range of the in-plane rotation. The novel suspension with approximately linear stiffness, which approximates the ideal special case $R/L = 0.87$ for straight beams, is shown in Fig. 1(a). A side view is shown in Fig. 2(a).

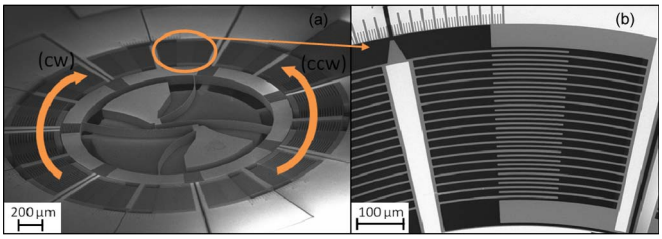

Fig. 2. (a) SE micrograph of the entire device with the arrows showing the cw and ccw directions, respectively. (b) Close-up SE micrograph of one set of comb fingers pulling the platform in the cw direction. The gauge used to measure the rotation can be seen at the top.

Furthermore, large-displacement static analysis is performed with finite-element modeling (FEM) in ANSYS to investigate the linearity of the spring. The simulated stiffness deviation from linearity was only 1.5% for up to $\pm 10^\circ$ mechanical rotation (corresponding to 40° optical scan angle), which is better than its counterparts in the literature [2], [5], [10].

III. Device Design and Fabrication

A 100-μm-thick MEMS rotary device is 3 mm in diameter. Two anchors are placed inside a circular stage [Fig. 1(a)]. Each anchor is connected to the ring through two 6-μm-wide flexures. To lower peak stresses, the corners of the flexures' connection points are rounded. Moreover, to each side of seven comb holders protruding from the ring, concentric comb actuators are attached. These are interdigitated with static comb fingers. The locations of the anchors and the shapes of the flexures were engineered to achieve high linearity.

In FEM, the rotary mode is estimated as 590 Hz. All higher modes are above 2500 Hz, well separated from the principal mode.

The microfabrication is performed with a three-mask process using silicon-on-insulator wafers with a highly doped 100-μm-thick device layer as starting material. The first fabrication step is to sputter and pattern 400 nm of Al to form the wire-bond electrodes as well as the measurement gauge. The front-side device structures and the back-side opening are then defined through photolithography and etched with deep reactive-ion etch (DRIE). After back-side DRIE to remove handle layer silicon from beneath the actuator, the devices are released by etch of the buried oxide in HF vapor. Since part of the actuator still sits on top of handle layer silicon, a few micrometers of side etch is needed to fully release the structure. Two SE micrographs of the MEMS device are shown in Fig. 2.

IV. Characterization

A. Drive Characteristics

The device is divided into three isolated potentials. The electrical connection to the rotational platform is achieved by wire bonds to the anchors. The static comb fingers driving the platform clockwise (cw) are all connected through the device layer silicon. Due to geometric necessity, the static comb fingers pulling the platform counterclockwise (ccw) are electrically isolated by isolation trenches and connected to each other with wire bonds [Fig. 1(b)].

B. Experimental Results

The present device's pull-in voltage of 40 V allowed for only 1° one-sided rotation for quasi-static actuation. Due to this limited deflection, the linearity of the stiffness could not be shown by nonresonant quasi-static actuation. In order to assess the rotational linearity, a collection

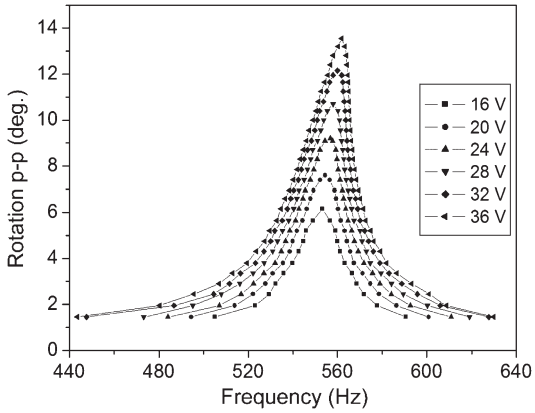

Fig. 3. Amplitude as a function of frequency at several voltage levels. Up to a peak-to-peak rotation of 10°, the frequency shift is less than 1%.

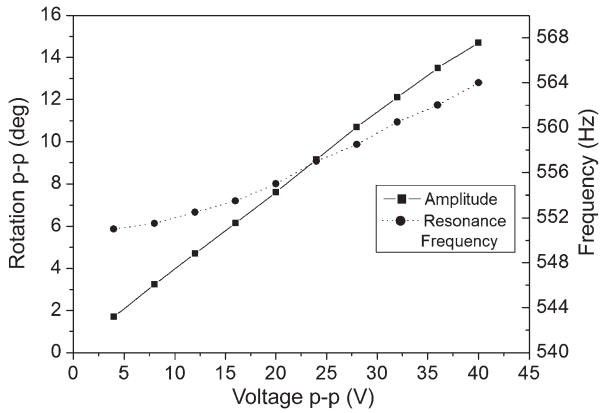

Fig. 4. Resonant deflection and resonant frequency as a function of excitation voltage. The frequency is adjusted at each voltage level to maximize the deflection. The rotation angle is measured via the imprinted scale.

of frequency response curves with various amplitude levels are taken at ambient pressure, as shown in Fig. 3. The resonant frequency is around 555 Hz, which is close to the FEM prediction. The peak value for each voltage was measured using a gauge and a scale imprinted on the device frame, as shown in Fig. 2(b). The scale has notches at every quarter degree, limiting the measurement resolution accordingly. Although there is little evidence of nonlinear spring stiffening with a slight resonance frequency shift of only about 1% up to 15° peak-to-peak rotation, these results clearly demonstrate a linear spring behavior well above that of conventional clamped–guided beams. There are no jump discontinuities in the frequency response, in contrast to other devices in the literature that use bending beams for a rotary suspension [2].

Fig. 4 shows the deflection at resonance as a function of voltage and the little change in resonance frequency with increased amplitude. The data are again taken by using the imprinted scale. In this experiment, the device is actuated with a differential drive voltage with an offset of 20 V. The resulting linear regression coefficient is larger than 0.99.

The device rotates more than $\pm 7^\circ$ when actuated with 40 V at ambient pressure. These tests safely prove that the spring design keeps linear stiffness for large rotation angles.

V. Conclusion and Future Work

A MEMS rotary stage featuring a bending flexure suspension with linear stiffness has been designed, fabricated, and characterized. The stiffness linearity is demonstrated by the insignificant shift in the

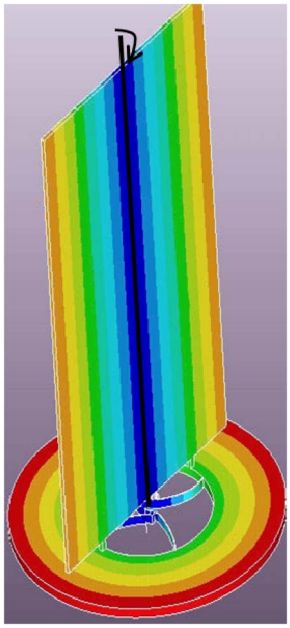

Fig. 5. Concept sketch with a mounted mirror.

resonance frequency of the rotational mode with increased angle and by the linear relation between rotational angle and voltage up to $\pm 7^{\circ}$ motion at resonance. Pull-in behavior is observed at relatively low voltages, which will be corrected in future devices by improved designs and use of wider comb fingers. A future application of this rotary stage is as an actuator for a quasi-static scanning mirror. A finite-element model of the envisioned device is shown in Fig. 5. The device is intended to be actuated quasi-statically at 60 Hz to enable its use as the slow-axis scanner for laser projection systems. Future work will focus on mounting a perpendicular mirror on top of the stage. The spring structure could also be implemented for precise control of valves in microfluidic applications or mounting various micro-optical, mechanical, or nanophotonic structures on the compact rotary stage and forming an array of such devices for beam steering and optical switching applications.

ACKNOWLEDGMENT

The microfabrication described in this letter was performed at the Center of Micronanotechnology, Ecole Polytechnique Federale de Lausanne, Lausanne, Switzerland. The authors would like to thank Y. Leblebici and P. Flückiger for their cooperation, M. Helsel for his help with the device fabrication, and S. Ölçer and E. Ermek for their help with the wire bonding and experiments.

REFERENCES

[1] U. Baran, W. O. Davis, S. Holmstrom, D. Brown, J. Sharma, S. K. Gokce, and H. Urey, "MEMS rotary stage with linear stiffness," in *Proc.IEEE/LEOS Int. Conf. Opt. MEMS Nanophoton.*, Istanbul, Turkey, 2010, pp. 37–38.

[2] Y. Du, G. Zhou, K. L. Cheo, Q. Zhang, H. Feng, and F. S. Chau, "A 2-DOF circular-resonator-driven in-plane vibratory grating laser scanner," *J. Microelectromech. Syst.*, vol. 18, no. 4, pp. 892–904, Aug. 2009.

[3] T. Juneau, A. Pisano, and J. H. Smith, "Dual axis operation of a micromachined rate gyroscope," in *Proc. Transducers*, Chicago, IL, 1997, vol. 2, pp. 883–886.

[4] T. Fujita, K. Maenaka, T. Mizuno, T. Matsuoka, T. Kojima, T. Oshima, and M. Maeda, "Disk-shaped bulk micromachined gyroscope with vacuum sealing," *Sens. Actuators A, Phys.*, vol. 82, no. 1–3, pp. 198–204, May 2000.

[5] J. D. Grade, K. Y. Yasumura, and H. Jerman, "Advanced, vibration-resistant, comb-drive actuators for use in a tunable laser source," *Sens. Actuators A, Phys.*, vol. 114, pp. 413–422, 2004.

[6] J. Grade and H. Jerman, "MEMS electrostatic actuators for optical switching applications," presented at the OSA Optical Fiber Communication Conf., Anaheim, CA, Mar., 2001, Paper WX2.

[7] J. A. Yeh, S. S. Jiang, and C. Lee, "MOEMS variable optical attenuators using rotary comb drive actuators," *IEEE Photon. Technol. Lett.*, vol. 18, no. 10, pp. 1170–1172, May 2006.

[8] T. C. Leïchlé, M. V. Arx, S. Reiman, I. Zana, W. Ye, and M. G. Allen, "A low-power resonant micromachined compass," *J. Micromech. Microeng.*, vol. 14, pp. 462–470, 2004.

[9] W. O. Davis, O. M. O'Reilly, and A. P. Pisano, "On the nonlinear dynamics of tether suspensions for MEMS," *J. Vib. Acoust.*, vol. 126, no. 3, pp. 326–331, Jul. 2004.

[10] J. A. Yeh, C. N. Chen, and Y. S. Lui, "Large rotation actuated by in-plane rotary comb-drives with serpentine spring suspension," *J. Micromech. Microeng*, vol. 15, no. 1, p. 201, Jan. 2005.

[11] A. H. Nayfeh, D. T. Mook, and P. Holmes, "Nonlinear oscillations," *J. Appl. Mech.*, vol. 47, p. 692, 1980.

[12] M. Stranczl, E. Sarajlic, G. J. M. Krijnen, H. Fujita, M. A. M. Gijs, and C. Yamahata, "Modal analysis and modeling of a frictionless electrostatic rotary stepper micromotor," in *Proc. IEEE Int. Conf. MEMS*, Cancun, Mexico, 2010, pp. 1257–1260.

[13] W. Davis, A. Pisano, and O. O'Reilly, "Nonlinear elastic coupling in tether-suspended MEMS," in *Proc. IEEE Int. Conf. MEMS*, Miami, FL, 2005, pp. 129–132.